PPP-derived High-Frequency Tropospheric Delays as a Measure of Atmospheric Turbulence

Markus Vennebusch[1], Steffen Schön[1] and Ulrich Weinbach[1,2]
[1]Institut für Erdmessung, Leibniz Universität Hannover, Germany
[2]Center for Quantum Optics and Space Research (QUEST), Leibniz Universität Hannover, Germany

Effects of atmospheric turbulence on GNSS observations

Atmospheric turbulence causes refractivity variations that can be observed in different steps of the geodetic data processing. For example, using high-frequency (1 Hz or more) GNSS carrier phase observations in a PPP analysis, high-frequency atmospheric effects can be observed as variations of estimated tropospheric zenith path delays or in post-fit carrier phase residuals (assuming low receiver noise, a stable receiver clock, and no multipath effects).

A common method to characterise fluctuations of both phase observations Φ and tropospheric delay estimates T is the (temporal) structure function (as a function of time lag t):

$$D_{\varphi}(t) = \langle [\Phi(x) - \Phi(x-t)]^2 \rangle \qquad (1)$$

Replacing the time lag t by a spatial distance d yields a spatial structure function. Double-logarithmic plots of structure functions of carrier phases and tropospheric delays typically show straight line segments that reveal the noise type of the corresponding stochastic process. Turbulence models predict a power-law behaviour with exponents (i.e., straight line slopes) ranging from 5/3 to 2/3 and finally 0.

Simulation of slant delay variations

A model of the impact of atmospheric turbulence on electromagnetic phase observations can be developed by using the geometrical optics approximation and by integrating refractivity variations along the line-of-sight from the receiver to the satellite (Wheelon, 2001). A covariance model for GNSS phase observations (and slant tropospheric delays) on the basis of the von Karman turbulence power spectrum has been developed by Schön/Brunner (2008) and reads (for parameter descriptions, see Tab. 1):

$$\langle T_A^i(t_A), T_B^j(t_B) \rangle = \frac{0.31\ \kappa_0^{-\frac{2}{3}}}{\sin\varepsilon_A^i \sin\varepsilon_B^j} C_n^2 \times \int_0^H \int_0^H (\kappa_0 d)^{\frac{1}{3}} K_{-\frac{1}{3}}(\kappa_0 d)\, dz_1\, dz_2 \qquad (2)$$

Equation (2) has to be solved numerically and can be used as a stochastic model for GNSS data analysis and for the simulation of tropospheric signal path variations (Vennebusch et al., 2010). Figure 1 shows simulation examples for a rising satellite.

Variable:	Description:	Variable:	Description:
$T_A^i(t_A)$	Slant tropospheric delay at station A to satellite i (at time t_A)	$T_B^j(t_B)$	Slant tropospheric delay at station B to satellite j (at time t_B)
C_n^2	Structure constant of refractivity n	ε_A^i	Elevation of satellite i at station A
$\kappa_0 = 2\pi/L_0$	Turbulence wavenumber corresponding to outer scale length L_0	d	Separation distance between actual integration points
$k = 2\pi/\lambda$	Electromagnetic wavenumber of signal wavelength λ	H	Height of wet troposphere ($\approx$ 2 km)
K	modified Bessel function of 2. kind		

Tab. 1: Parameter descriptions for covariance model (Eq. (2)).

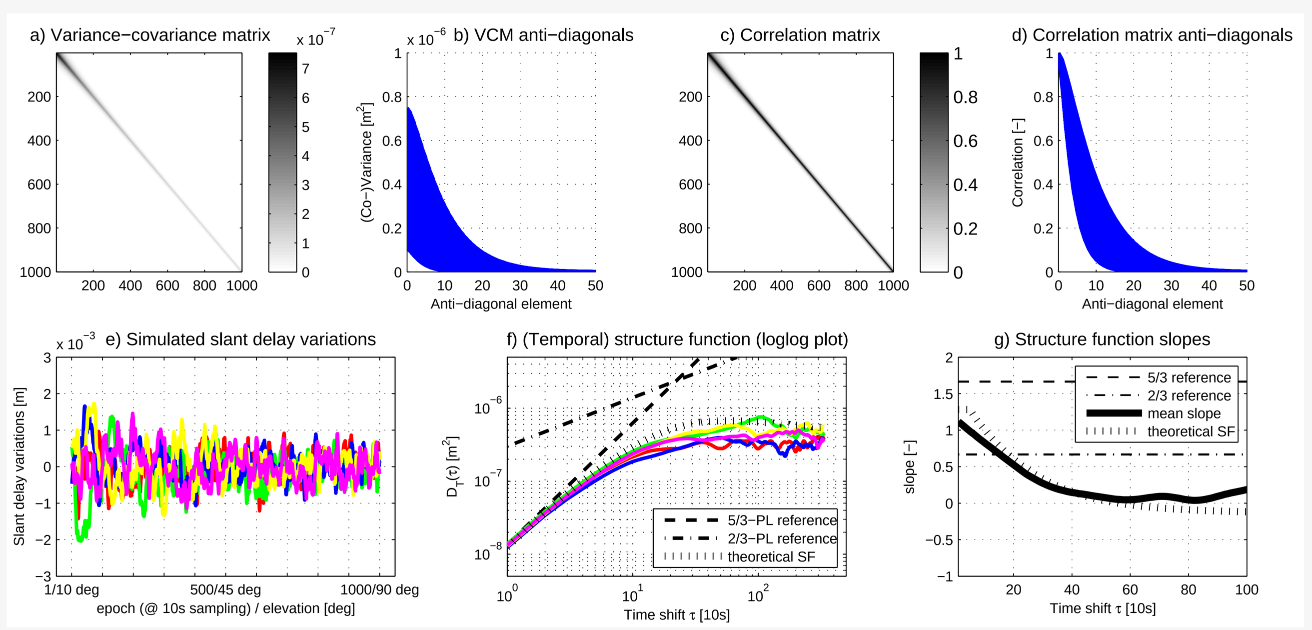

Fig. 1: Variance-covariance matrix, correlation matrix, anti-diagonal values, simulated slant delay time series, temporal structure functions and their slopes for a satellite rising from 10° to 90° elevation (for typical conditions of atmospheric turbulence).

PPP: Zenith tropospheric delays

Using specially designed GPS networks, both temporal and spatial characteristics of atmospheric turbulence can be studied. As an example, figure 2 shows the so-called Seewinkel network of six equally equipped L1/L2-GPS-receivers located along a 16 km straight line. Both pseudorange and carrier phase data has been recorded for approximately eight hours with a sampling interval of 30 s.

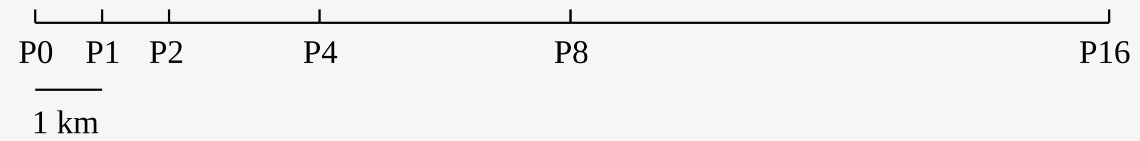

Fig. 2: Seewinkel network geometry (6 Leica SR530/520 receivers with choke ring antennas with SCIS radomes located along a 16 km straight line, maximum height difference: 10 m).

Using PPP, this data has been processed to derive high-frequency zenith tropospheric path delays (for settings, see Tab. 2). These time series were used to generate temporal and spatial structure functions shown in figures 3 and 4. The temporal characteristics shows a power-law behaviour with a smooth transition between exponents of 5/3, 2/3 and finally 0.

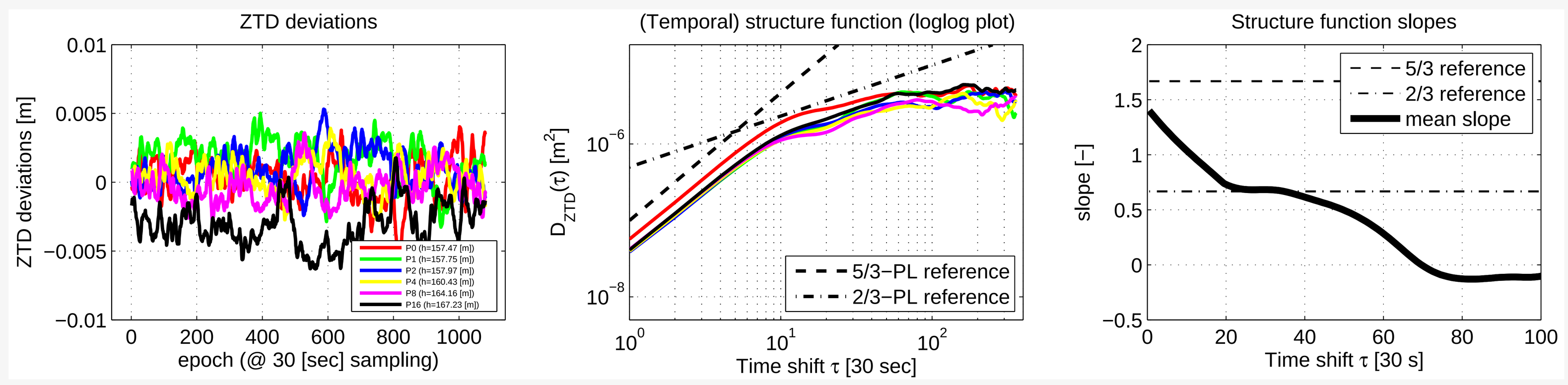

Fig. 3: Temporal characteristics of PPP tropospheric signal delays. The estimated ZTD deviations show peak-to-peak variations of up to 5 mm. The temporal structure functions indicate an initial power-law behaviour of almost 5/3 for the first approximately 10 epochs (300 s) and a slope of approximately 2/3 for time shifts of 10 to 50 epochs (300 to 1500 s). After approximately 70 epochs (2100 s) the estimated ZTD deviations can be considered as uncorrelated.

The spatial characteristics follows a 2/3-power law behaviour, i.e. the station separation is large compared to the effective tropospheric height so that the turbulence process can be considered as two-dimensional.

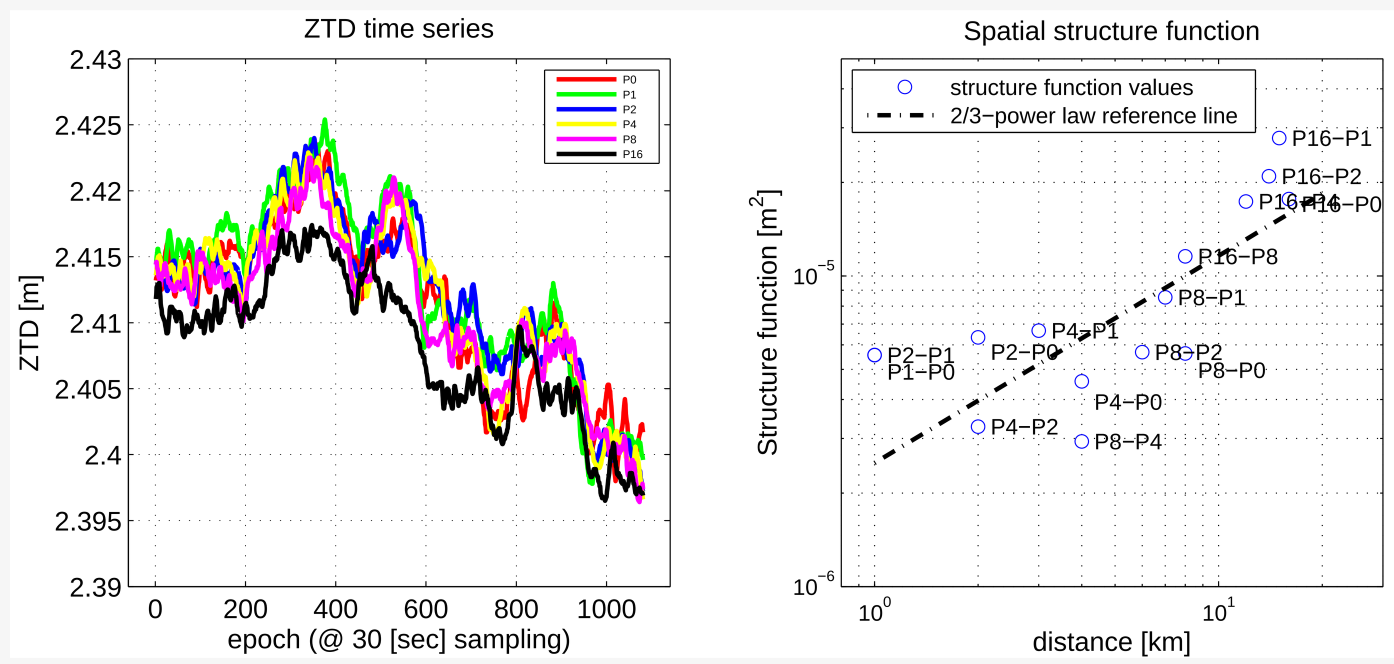

Fig. 4: Spatial characteristics of PPP tropospheric signal delays.

Elevation cut-off	10°
Sampling	30 s
Satellite orbits	MI112142.SP3 (15 min, reprocessing campaign)
Satellite clocks	MI112142.CLK (30 s, reprocessing campaign)
Troposphere modelling	random walk with process noise of 15 mm/$\sqrt{h}$
Antenna PCV	absolute PCV, from IGS05.atx

Tab. 2: PPP analysis settings.

PPP: Carrier phase residuals

In addition, refractivity variations can be observed in the raw carrier phase observations (Wheelon, 2001). Since undifferenced carrier phase observations contain superpositions of several effects (such as residual receiver clock variations, receiver noise, multipath and turbulence effects) the separation of these effects is a challeging task.

In order to investigate the different effects, Seewinkel network carrier phase observations (derived from the internal quartz oscillator) have been compared to carrier phase observations of IGS stations connected to hydrogen masers. Fig. 5 and 6 show examples of PPP post-fit residuals and their temporal structure functions together with estimated receiver clock offsets.

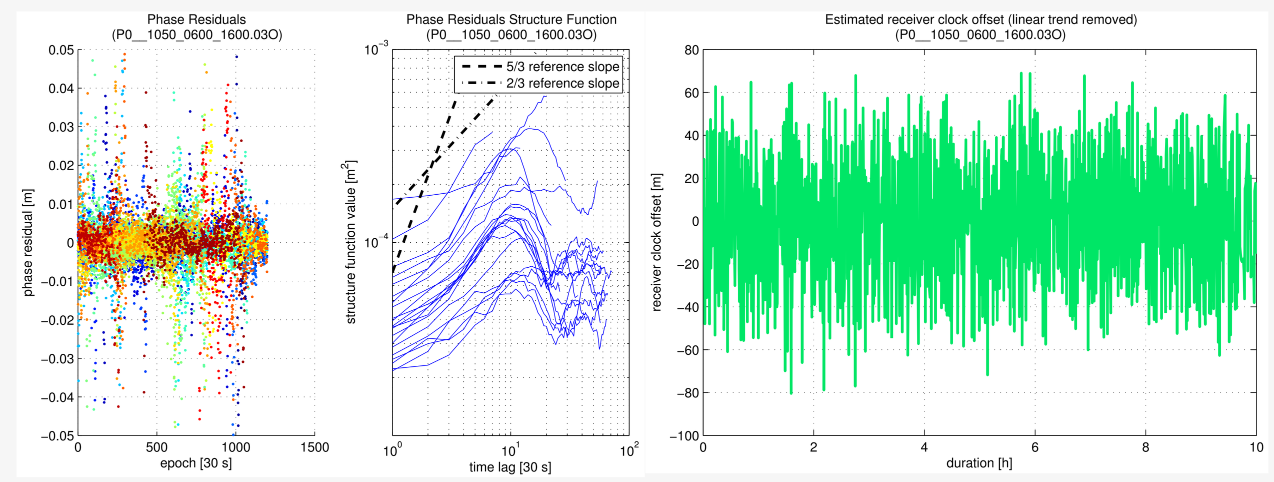

Fig. 5: Seewinkel station P0 (internal quartz oscillator): PPP carrier phase residuals, their temporal structure functions and estimated receiver clock offsets.

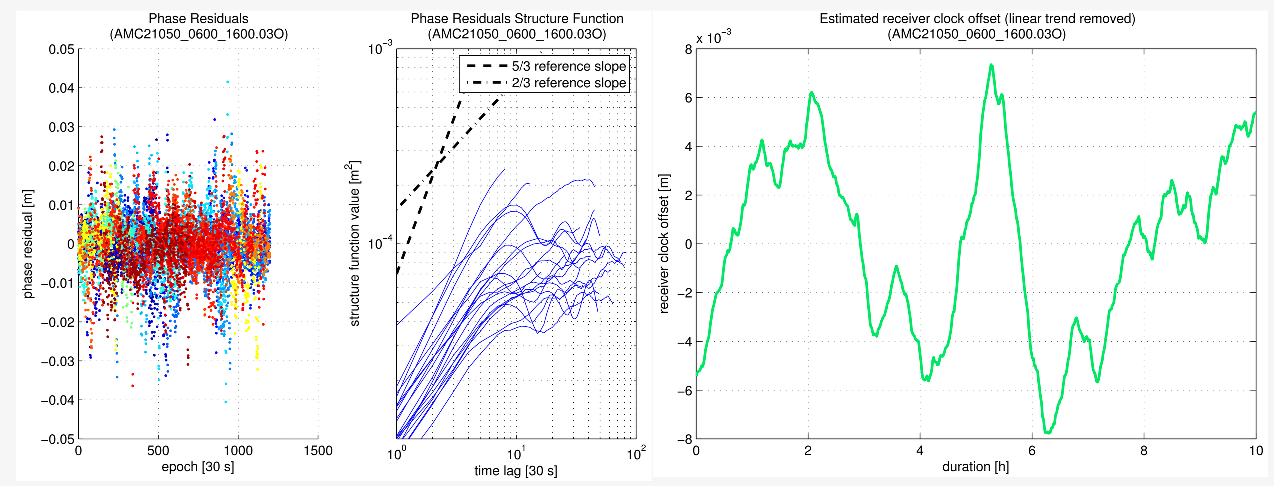

Fig. 6: IGS station AMC2 (hydrogen maser): PPP carrier phase residuals, their temporal structure functions and estimated receiver clock offsets.

Carrier phase structure functions (cf. Eq. (1)) show the different noise types of the underlying time series: Structure function values for short time lags τ (i.e., the beginning of the structure function) indicate the amount of short periodic white noise, while for large time lags τ the structure function approaches twice the variance of the original signal (Wheelon, 2001).

Comparisons of Fig. 5 and 6 show the presence of remaining short-periodic effects in the carrier phase residuals of station P0 that flattens the slope for small time lags (stations P1 to P16 show similar behaviour). Candidates for these effects might be remaining receiver clock effects or receiver dependent noise. Further investigations/experiments will concentrate on the separation of these effects and on the detection of atmospheric turbulence.

References & Acknowledgements

Schön S, Brunner FK: Atmospheric turbulence theory applied to GPS carrier-phase data, J Geod 82(1): 47-57, 2008.
Thompson AR, Moran JM, Swenson GW: Interferometry and Synthesis in Radio Astronomy, Wiley, 2004.
Vennebusch M, Schön S, Weinbach U: Temporal and spatial stochastic behaviour of high-frequency slant tropospheric delays from simulations and real GPS data, Advances in Space Research, Special Issue: GNSS Remote Sensing, Elsevier, 2010.
Wheelon AD: Electromagnetic scintillation-I. Geometrical optics, Cambridge University Press, Cambridge, 2001.

The authors thank the German Research Foundation (Deutsche Forschungsgemeinschaft) for its financial support (SCHO 1314/1-1) and Fritz K. Brunner (IGMS, TU Graz) for the permission to use the Seewinkel data in this study.

Institut fur Erdmessung
Schneiderberg 50
D-30167 Hannover

EGU 2011
3 - 8 April 2011

Markus Vennebusch
Steffen Schön, Ulrich Weinbach
www.ife.uni-hannover.de
{vennebusch, schoen, weinbach}@ife.uni-hannover.de